Recessive *DNAH9* Loss-of-Function Mutations Cause Laterality Defects and Subtle Respiratory Ciliary-Beating Defects

Niki T. Loges,[1,13] Dinu Antony,[2,3,13] Ales Maver,[4] Matthew A. Deardorff,[5,6] Elif Yýlmaz Güleç,[7] Alper Gezdirici,[7] Tabea Nöthe-Menchen,[1] Inga M. Höben,[1] Lena Jelten,[1] Diana Frank,[1] Claudius Werner,[1] Johannes Tebbe,[1] Kaman Wu,[2] Elizabeth Goldmuntz,[5,8] Goran Čuturilo,[9] Bryan Krock,[10,11] Alyssa Ritter,[6,8] Rim Hjeij,[1] Zeineb Bakey,[2,3] Petra Pennekamp,[1] Bernd Dworniczak,[1] Han Brunner,[2] Borut Peterlin,[4] Cansaran Tanidir,[12] Heike Olbrich,[1] Heymut Omran,[1,13,*] and Miriam Schmidts[2,3,13,*]

Dysfunction of motile monocilia, altering the leftward flow at the embryonic node essential for determination of left-right body asymmetry, is a major cause of laterality defects. Laterality defects are also often associated with reduced mucociliary clearance caused by defective multiple motile cilia of the airway and are responsible for destructive airway disease. Outer dynein arms (ODAs) are essential for ciliary beat generation, and human respiratory cilia contain different ODA heavy chains (HCs): the panaxonemally distributed γ-HC DNAH5, proximally located β-HC DNAH11 (defining ODA type 1), and the distally localized β-HC DNAH9 (defining ODA type 2). Here we report loss-of-function mutations in *DNAH9* in five independent families causing situs abnormalities associated with subtle respiratory ciliary dysfunction. Consistent with the observed subtle respiratory phenotype, high-speed video microscopy demonstrates distally impaired ciliary bending in *DNAH9* mutant respiratory cilia. *DNAH9*-deficient cilia also lack other ODA components such as DNAH5, DNAI1, and DNAI2 from the distal axonemal compartment, demonstrating an essential role of DNAH9 for distal axonemal assembly of ODAs type 2. Yeast two-hybrid and co-immunoprecipitation analyses indicate interaction of DNAH9 with the ODA components DNAH5 and DNAI2 as well as the ODA-docking complex component CCDC114. We further show that during ciliogenesis of respiratory cilia, first proximally located DNAH11 and then distally located DNAH9 is assembled in the axoneme. We propose that the β-HC paralogs DNAH9 and DNAH11 achieved specific functional roles for the distinct axonemal compartments during evolution with human DNAH9 function matching that of ancient β-HCs such as that of the unicellular *Chlamydomonas reinhardtii*.

Cilia are hair-like organelles that project from the surface of nearly all polarized cell types, fulfilling essential roles in cellular signaling and motility.[1] The basic structure of cilia is remarkably conserved throughout evolution. Most motile cilia consist of a ring of nine peripheral microtubule doublets that surrounds a central pair (CP) of single microtubules (9+2 structure). Motile monocilia at the mouse node transiently present during early embryogenesis are an exception, lacking the central pair apparatus (9+0 structure). Distinct multi-protein dynein complexes attached at regular intervals to the peripheral microtubule doublets contain molecular motors that drive and regulate ciliary motility. The inner dynein arms (IDAs) and the nexin link-dynein regulatory complexes (N-DRCs) regulate ciliary and flagellar beating pattern and frequency, while radial spoke (RS) complexes connect the CP apparatus with the nine peripheral microtubules.[2]

The outer dynein arms (ODAs) are responsible for the ciliary beat generation. ODAs and IDAs are large multimeric protein complexes that are pre-assembled in the cytoplasm before transport to the axonemes.[3] In the unicellular alga *Chlamydomonas reinhardtii*, there is only one type of ODA which contains three dynein heavy chains: the α-dynein heavy chain (DHC), the β-DHC, and the γ-DHC.[4] In contrast, in mammalian respiratory cilia, there are at least two types of ODAs, the ODA type 1 containing DNAH5 (ortholog of the γ-DHC) as well as DNAH11 (ortholog of the β-DHC) and the ODA type 2 containing DNAH5 and DNAH9 (also ortholog of the β-DHC). Using immunofluorescence analysis of human respiratory epithelial cells, we demonstrated in the past that the ODA heavy chains (HCs) show specific localization along the respiratory ciliary axonemes. The γ-HC DNAH5 shows a panaxonemal distribution along the ciliary axonemes. In

[1]Department of General Pediatrics, University Hospital Muenster, 48149 Muenster, Germany; [2]Genome Research Division, Human Genetics Department, Radboud University Medical Center and Radboud Institute for Molecular Life Sciences, Geert Grooteplein Zuid 10, 6525KL Nijmegen, the Netherlands; [3]Center for Pediatrics and Adolescent Medicine, University Hospital Freiburg, Freiburg University Faculty of Medicine, Mathildenstrasse 1, 79112 Freiburg, Germany; [4]Clinical Institute of Medical Genetics, UMC Ljubljana, Šlajmerjeva 4, 1000 Ljubljana, Slovenia; [5]Departments of Pediatrics and Pathology, The Perelman School of Medicine, University of Pennsylvania, Philadelphia, PA 19104, USA; [6]Laboratory Medicine, The Perelman School of Medicine, University of Pennsylvania, Philadelphia, PA 19104, USA; [7]Department of Medical Genetics, University of Health Sciences, Kanuni Sultan Suleyman Training and Research Hospital, 34303 Istanbul, Turkey; [8]Division of Human Genetics, Children's Hospital of Philadelphia, Philadelphia, PA 19104, USA; [9]Department of Medical Genetics, University Children's Hospital, 11000 Belgrade, Serbia; [10]Division of Cardiology, Children's Hospital of Philadelphia, Philadelphia, PA 19104, USA; [11]Division of Genomic Diagnostics, Children's Hospital of Philadelphia, Philadelphia, PA 19104, USA; [12]University of Health Sciences, Mehmet Akif Ersoy Thoracic and Cardiovascular Surgery Training and Research Hospital, Department of Pediatric Cardiology, 34303 Istanbul, Turkey
[13]These authors contributed equally to this work
*Correspondence: heymut.omran@ukmuenster.de (H.O.), miriam.schmidts@uniklinik-freiburg.de (M.S.)
https://doi.org/10.1016/j.ajhg.2018.10.020.
© 2018 The Author(s). This is an open access article under the CC BY-NC-ND license (http://creativecommons.org/licenses/by-nc-nd/4.0/).

contrast, the localization of the β-HC DNAH9 is restricted to the distal axonemal compartment while the paralogous β-HC DNAH11 is localized in the proximal axonemal compartment.[5,6] Thus, the human respiratory ciliary axoneme can be divided in two compartments, a proximal compartment defined by the ODA type 1 (containing DNAH11) and a distal compartment defined by the ODA type 2 (containing DNAH9). The identification of genes that encode for proteins responsible for correct composition and assembly of these distal and proximal protein complexes is critical to understand the disease mechanisms of motile ciliopathies such as primary ciliary dyskinesia (PCD).

Primary ciliary dyskinesia (MIM: 244400) is a rare genetic disorder affecting approximately 1 in 20,000 individuals and is caused by immotile or dyskinetic cilia. Defective ciliary function in upper and lower airways causes defective mucociliary airway clearance and subsequently chronic inflammation that regularly progresses to destructive airway disease (bronchiectasis). Established diagnostic tools include measurement of nasal nitric oxide (NO) production rate (most often found to be low, distinguishing PCD from other chronic destructive airway diseases), structural ciliary analyses for motility apparatus components using transmission electron microscopy (TEM) or high-resolution immunofluorescence microscopy (IF), and analysis of ciliary beating by high-speed videomicroscopy (HVSM).[7,8] Furthermore, dysfunctional sperm tails (flagella), a special type of motile cilia, can cause male infertility in PCD-affected individuals if the genetic defects also affect the composition or function of sperm flagella. Organ laterality defects are also observed with approximately half of PCD individuals exhibiting situs inversus totalis, where left-right visceral organ positions are completely inverted. Other laterality defects are less frequently observed in PCD and are summarized under the term situs ambiguous (SA) represented by conditions such as situs inversus of only one body cavity (thoracalis or abdominalis), right isomerism associated with asplenia, or left isomerism associated with polysplenia.[9,10] Congenital heart defects can also represent manifestations of SA including transposition of the great arteries or hypoplastic left heart.[11]

Left-right patterning in humans, as in other mammals, is determined in the early embryo and greatly depends on proper functioning of the embryonic node. In 1998, Nonaka et al. demonstrated that motile monocilia transiently present at the embryonic node produce a leftward fluid flow that is essential for correct determination of left-right body asymmetry.[12] Two models have been proposed to explain how nodal flow might contribute to the start of the asymmetric nodal signaling cascade important for the establishment of left-right body asymmetry. The "two-cilia" model predicts that there are two distinct types of cilia and that nodal flow is generated by motile monocilia of pit cells and sensed by non-motile, mechanosensory monocilia of crown cells at the periphery of the node.[13] The "morphogen gradient" model predicts that the nodal flow results in a leftward gradient of a hypothetical morphogen. Tanaka et al. identified nodal vesicular parcels that bud off the nodal surface to be transported leftward by nodal flow where they are smashed to release their contents.[14] In both cases, motility of node monocilia is essential to generate the leftward nodal flow important to initiate the asymmetric nodal signaling cascade to establish laterality.

Therefore, human laterality defects can be caused by mutations in genes encoding proteins important for the integrity of the ciliary motility apparatus, resulting in impaired ciliary motility and subsequent impaired or disturbed leftward fluid flow within the embryonic node. In addition, laterality defects can occur in non-motility-related ciliopathies, for example due to mutations in *Inversin*[15] (MIM: 243305), *PKD1L1*[16,17] (MIM: 609721), *PKD2*[18,19] (MIM: 607074), or *NPHP3*[20] (MIM: 608002), where non-motile mechano-sensory monocilia at the margin of the embryonic node are thought to be defective. In addition, signals at the node are also further processed without the involvement of cilia. As a consequence, laterality defects are also observed due to defects in genes encoding non-ciliary proteins, e.g., due to mutations in *ZIC3*[21] (MIM: 300265), *ACVR2B*[22] (MIM: 602730), *NODAL*[23] (MIM: 601265), *GDF1*[24] (MIM: 602880), or *MMP21*[25] (MIM: 608416).

To date, mutations in more than 35 genes associated with PCD and mucociliary clearance disorders have been identified; however, these still explain only about two thirds of all human cases.[26,27] Among the most common causes are lack of ODAs and nearly 20% of all PCD-affected case subjects result from mutations in *DNAH5* (MIM: 603335), which encodes the axonemal ODA γ-HC DNAH5.[28] Other genes found to carry PCD-causing variants and resulting in ODA defects include *DNAI1* (MIM: 604366) and *DNAI2* (MIM: 605483), which encode the axonemal ODA intermediate chains 1 and 2, respectively.[29,30] Loss of function of *DNAH5* results in PCD with complete or nearly complete ciliary immotility and complete axonemal loss of ODAs observed by TEM. In contrast, loss-of-function of *DNAH11* (MIM: 603339) results in a PCD phenotype with apparently normal ciliary ultrastructure by TEM but abnormal hyperkinetic ciliary beating pattern with reduced proximal bending depicted by HSVM.[6,31,32]

As mutations in the genes encoding axonemal ODA HCs such as DNAH5[33] and DNAH11[31,32] are very common in PCD-affected individuals, we expected also to identify mutations in *DNAH9* (MIM: 603330) in PCD-affected individuals with ODA defects or normal ciliary ultrastructure as well as individuals with laterality defects. Therefore, we used a customized PCD gene panel (Table S1) for targeted next generation sequencing (NGS), whole-exome sequencing (WES), as well as Sanger sequencing of *DNAH9* (GenBank: NM_001372.3) to screen individuals with classical PCD symptoms fulfilling the diagnostic criteria of the European Respiratory Society (ERS)[34] as

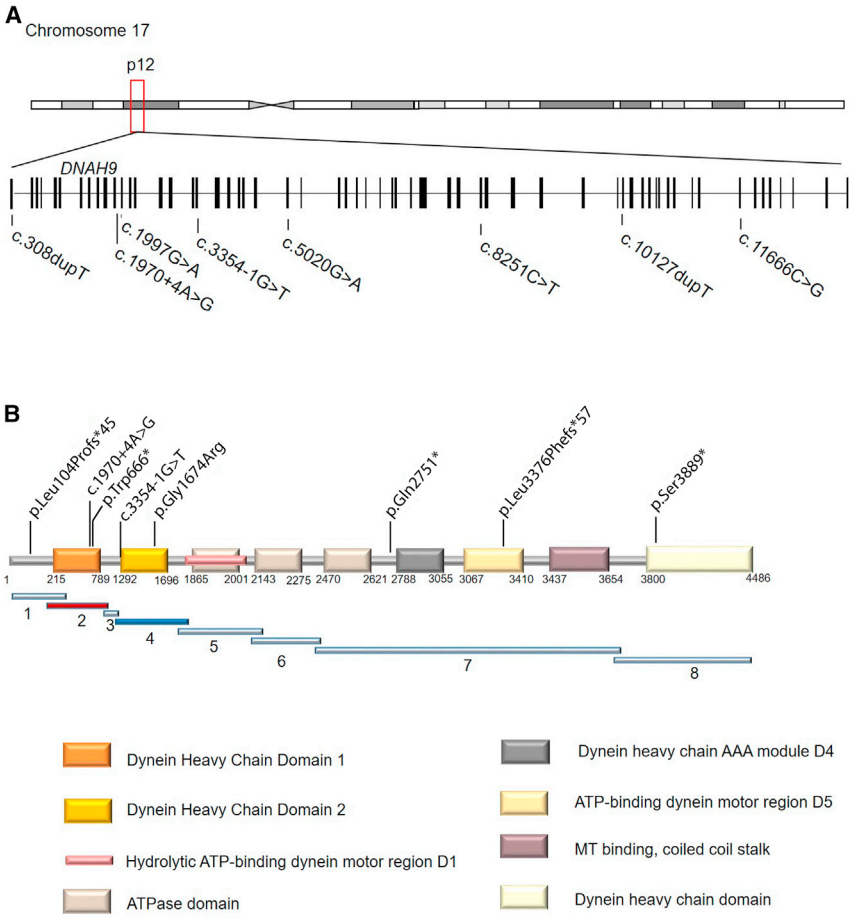

Figure 1. *DNAH9* Mutations in Individuals with Laterality Defects and/or Mild Respiratory Symptoms

(A) Schematic presentation of chromosome 17 and the exon-intron structure of *DNAH9*. The positions of the eight mutations identified in five unrelated families are indicated. (B) Predicted protein model of DNAH9 with the distinct domains and indication of DNA fragment distribution for protein-protein interaction experiments.

well as individuals with laterality defects and only mild or no respiratory symptoms, not fulfilling ERS PCD criteria. Of 548 individuals screened in total, 138 individuals were classified to have PCD with ODA defects, 255 individuals suspected to have PCD with normal ciliary structure documented by IF and/or TEM, 99 individuals suspected to have PCD without any information on the ciliary structure, 12 individuals with mild respiratory symptoms and ciliary beating defects documented by HSVM without laterality defects, and 44 individuals with laterality defects and mild or no respiratory symptoms (Figure S1). 85 individuals were screened by direct Sanger sequencing of *DNAH9*, 421 individuals were analyzed using a targeted gene panel containing all known PCD genes as well as laterality defect candidate genes including *DNAH9* (Table S1), and 42 individuals were analyzed by WES (Figure S1). A detailed description of sequencing methods including gene panel composition is included in the Supplemental Methods. DNA samples were collected after obtaining informed consent from affected individuals or parents as part of the clinical diagnostic pathway at Radboud UMC Nijmegen (Innovative diagnostic program) or as part of a research study with the approval of the Institutional Ethics Review Board at the University of Muenster.

Using this combined approach, interestingly we did not identify biallelic *DNAH9* variants in any individual fulfilling ERS PCD diagnostic criteria; however, we identified two splice site variants c.1970+4A>G and c.3354−1G>T in *DNAH9* in individual OP-2905 II1 who presented with situs inversus totalis and only mild respiratory symptoms using the PCD gene panel sequencing approach (Figures 1, S2A, and S2B and Table 1). Both variants are predicted to affect splicing and to result in aberrant transcripts. Unfortunately, no cells from OP-2905 II1 were available for mRNA analyses. For this reason, we used the SpliceSite Finder-like, MaxEntScan, NNSPLICE, GeneSplicer, and the Human Splice Finder software available through Alamut to analyze both variants. Alamut software predicts variant c.1970+4A>G to result in a novel splice site 4 bp downstream in the intron (score 82.6) not present in the wild-type DNA sequence while scores for the wild-type splice positions are moderately reduced (Figure S3). Additionally, Alamut predicts that the variant c.3354−1G>T leads to abrogation of the splice site as expected for a mutation affecting a consensus splice position which is predicted to result in loss of exon 18 (223 bp) and subsequent frameshift (Figure S3). Based on this finding, we analyzed additional individuals with laterality defects and mild or no respiratory symptoms (n = 43) not fulfilling classical PCD diagnostic criteria as defined by the ERS consensus statement[34] and individuals without laterality defects and only mild respiratory symptoms (n = 12) associated with subtle ciliary-beating defects likewise, using direct Sanger sequencing of *DNAH9* (n = 1), targeted gene panel sequencing (n = 12), or whole-exome sequencing (WES) (n = 42) datasets (Figure S1). Sequencing methods and filtering strategies are described in detail in the Supplemental Methods.

This sequencing strategy resulted in the identification of two additional individuals with laterality defects carrying biallelic *DNAH9* (GenBank: NM_001372.3) loss-of-function alleles, a homozygous nonsense mutation in individual OP-1226 II1 (c.8251C>T [p.Gln2751*]) identified using Sanger sequencing, and a homozygous frameshift variant

Table 1. Clinical, Diagnostic, and Genetic Findings in *DNAH9* Mutant Individuals

	OP-2905 II1	OP-1226 II1	MS-SI46 II1	AM II1	MD II1
Origin	Germany	Germany	Turkey	Serbia	USA
Consanguinity	no	no	yes	no	no
Respiratory phenotype	mild	none	mild	N/A	mild
nNO	76 nL/min (230 ppb)	106 nL/min (321 ppb) (2011) 67 nL/min (202 ppb) (2015)	N/A	N/A	N/A
HVSM	reduced distal bending	reduced distal bending	N/A	N/A	N/A
TEM	partial absence of ODAs	N/A	N/A	N/A	N/A
IF	absence of DNAH9 and distal absence of DNAI1, DNAI2, DNAH5; DNAH11 normal	absence of DNAH9 and distal absence of DNAI1, DNAI2, DNAH5; DNAH11 normal	absence of DNAH9 and distal absence of DNAI1, DNAI2, DNAH5	N/A	N/A
Laterality defect	situs inversus totalis	situs inversus totalis	situs inversus totalis	situs ambiguous with complex heart defect (left atrial isomerism, atrioventricular canal defect, interrupted vena cava inferior, anomalous pulmonary vein connection, persistent ductus arteriosus)	heterotaxy with situs inversus, interrupted inferior vena cava with azygous continuation, right aortic arch with mirror image head and neck vessel branching, liver and gall bladder on left, multiple splenules on right side
Other features	septo-optic dysplasia	none	none	died at 8 days of age due to cardiac defect	hydrocephalus and a ventriculoperitoneal shunt after group B streptococcal sepsis as infant
DNAH9 alleles	c.1970+4A>G + c.3354−1G>T	c.8251C>T (p.Gln2751*) (homozygous)	c.10127dupT (p.Leu3376Phefs*57) (homozygous)	c.308dupT (p.Leu104Profs*45) + c.11666C>G (p.Ser3889*)	c.1997G>A (p.Trp666*) + c.5020G>A (p.Gly1674Arg)
Sequencing technology used for primary variant identification	NGS targeted gene panel (see Table S1 for details)	Sanger sequencing	WES (SureSelect V6 whole exome kit)	NGS Illumina Trusight One targeting 12 Mb panel	clinical WES (Agilent SureSelect XT Clinical Research Exome kit)

Abbreviations: N/A, not available; NGS, next generation sequencing; ODA, outer dynein arm; WES, whole-exome sequencing.

c.10127dupT (p.Leu3376Phefs*57) detected by WES in individual MS-SI46 II1 (Figures 1, S2A, and S2B and Table 1). All remaining WES variants after filtering the NGS data of individual MS-SI46 II1 are shown in Table S2. Variants in *DNAH9* were prioritized due to the fact that *DNAH9* encodes an axonemal dynein heavy chain involved in ciliary motility and because loss of function of *DNAH9* causes situs inversus totalis as observed in OP-2905 II1. Subsequently, using the GeneMatcher Database (Figure S1), we found two additional independent cases with laterality defects and biallelic loss-of-function variants in *DNAH9*: AM II1 carrying c.308dupT (p.Leu104Profs*45) and c.11666C>G (p.Ser3889*) and MD II1 found to carry c.1997G>A (p.Trp666*) and c.5020G>A (p.Gly1674Arg) (Figures 1, S2A, and S2B and Table 1). Next generation sequencing techniques applied for these two individuals, namely NGS Illumina Trusight One targeting 12 Mb panel used for individual AM II1 and clinical WES for individual AM II1, are described in detail in the Supplemental Methods.

We confirmed all variants identified by different NGS methods using Sanger sequencing (primer sequences available on request), including variant segregation within families where parental DNA was available (Figure S2). Consistent with previously identified PCD-causing variants in other genes, seven of eight *DNAH9* mutant alleles represent putative null alleles including nonsense, frameshift, or splice site variants. The c.5020G>A (p.Gly1674Arg) missense variant identified in a compound heterozygous state along with a nonsense mutation in individual MD II1 affects an evolutionarily highly conserved amino acid and is predicted to be damaging by MutationTaster and PolyPhen-2 (Figure S4). The variant exchanges a small neutral amino acid (glycine) for a larger, positively charged amino acid (arginine) and the variant is located within the second DHC domain of DNAH9 (Figure 1). The amino acid exchange is likely to disrupt secondary protein structures due to size and charge differences (prediction by HOPE, data not shown). In summary, we identified eight different variants in *DNAH9* in five individuals with laterality defects from five independent families of which one is a missense allele affecting a highly conserved amino acid while the seven remaining represent putative null alleles. Four variants (c.3354−1G>T, c.8251C>T [p.Gln2751*], c.10127dupT [p.Leu3376Phefs*57], and c.1997G>A [p.Trp666*]) are not present in the Genome Aggregation Database and four variants are present with very low-allele frequencies (c.1970+4A>G: 0.0001488; c.308dupT [p.Leu104Profs*45]: 0.0002637; c.11666C>G [p.Ser3889*]: 7,223e−6, and c.5020G>A [p.Gly1674Arg]: 1.627e−5).

None of the five individuals harboring biallelic *DNAH9* mutant variants were clinically diagnosed with PCD (Table 1). However, mild respiratory symptoms including frequent cold-like infections were observed in individuals OP-2905 II1, MS-SI46 II1, and MD II.1. The nasal NO production rate was measured 76 nL/min for OP-2905 II1 (one occasion) and 106 nL/min (first occasion, 2011) and 67 nL/min (second occasion, 2015) for OP-1226 II1 using the EcoMedics CLD88 (EcoMedics) system. Thus, the nasal NO production rate was in the low range but above the cut-off value for PCD previously reported by most studies (30–52.5 nL/min)[35,36] and only minimally below the cut-off value reported in two other studies (77 nL/min and 82 nL/min)[37,38] used for PCD screening.

All five individuals presented laterality defects (Table 1). Additionally, individual OP-2905 II1 displayed a midline defect of septo-optic dysplasia. However, we believe the midline defect in OP-2905 II1 may not necessarily be related to the detected *DNAH9* mutations. Individuals OP-2905 II1, OP-1226 II1, and MS-SI46 II1 displayed situs inversus totalis (Figure 2A), AM II1 presented with situs ambiguous with complex congenital heart defects, including left atrial isomerism, atrioventricular canal defect, interrupted vena cava inferior, anomalous pulmonary vein connection, and persistent ductus arteriosus that caused fatal cardiorespiratory failure in the early neonatal period. Individual MD II1 was diagnosed with heterotaxy with situs inversus and polysplenia. Thus, our data indicate that *DNAH9* mutations cause laterality defects with no or only mild respiratory symptoms such as recurrent airway infections instead of a classical respiratory PCD phenotype. Fertility is often reduced in classical PCD, but none of the individuals reported here carrying biallelic *DNAH9* variants has reached reproductive age yet. Clinical features and results of further investigations of cilia function and ciliary ultrastructure are summarized in Table 1.

We identified laterality defects as the leading clinical feature in individuals with loss of function of *DNAH9* (Table 1 and Figure 2A). The ventral embryonic node is the left-right organizing center in mammals. Coordinated beating of nodal monocilia plays a crucial role for establishment of correct laterality by establishing a leftward flow essential for activation of the left-right signaling cascade (Figure 2B). We therefore hypothesized that DNAH9 could be involved in node monocilia function and proceeded to perform *in situ* hybridization analyses of wild-type mouse embryos (0 somite stage) as previously described.[39] The exact developmental stage of mouse embryos was determined by morphological landmarks or the number of somites.[40] A 529 bp fragment of mouse *Dnah9* (GenBank: NM_001099633.1) cDNA was amplified from wild-type mouse fallopian tube cDNA and subsequently ligated into pCRII-TOPO vector by TOPO cloning reaction (Invitrogen, Thermo Fisher Scientific). After hybridization with the antisense probe, we detected a strong signal with the antisense probe located to pit cells of the node, but not in crown cells of the node (Figure 2C). In contrast, no signal was observed using the sense probe as a negative control (Figure 2C). These findings are consistent with *DNAH9* involvement in the function of motile node monocilia and that loss of DNAH9 causes an impairment of nodal ciliary beating and subsequently altered nodal flow, to result in laterality defects. Although all

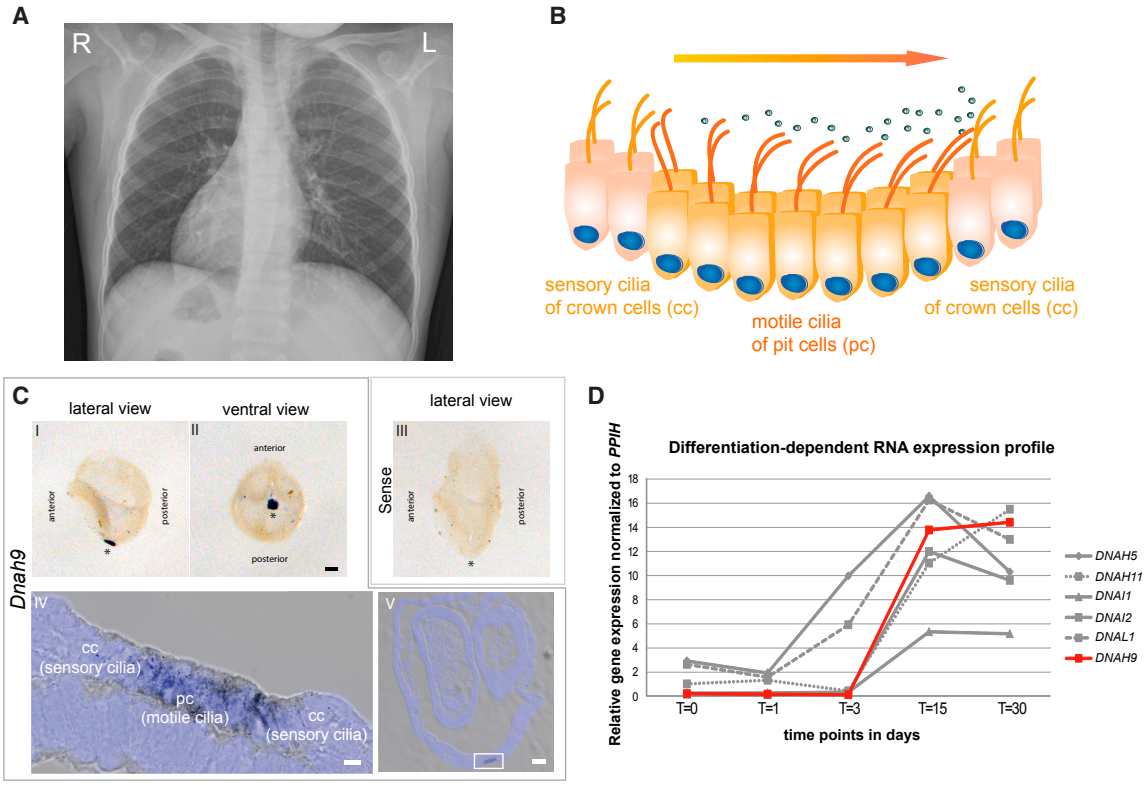

Figure 2. *Dnah9* Is Essential for Determination of Left-Right Body Asymmetry and Is Expressed in Nodal Cells Carrying Motile Nodal Monocilia Important to Generate the Nodal Flow

(A) The chest X-ray radiograph of MS-SI46 II1 depicts situs inversus totalis.

(B) Schematic of the "two cilia" nodal flow hypothesis. Motile cilia of the pit cells (pc) generate a leftward nodal fluid flow which is sensed by the sensory cilia of the crown cells (cc), which is necessary to start the signaling cascade to establish correct left-right body asymmetry.

(C) *In situ* hybridization analyses in wild-type mouse embryos show specific expression of *Dnah9*. Lateral (I) and ventral (II) view of a 0 somite wild-type mouse embryo demonstrate that *Dnah9* expression is restricted exclusively to the left-right organizer (LRO) as indicated by the spot like dark blue signal. (III) Sense probe does not show any specific staining (I-III). Asterisks indicate the position of the LRO. Scale bars represent 100 μm. (IV) *Dnah9* expression indicated by the grayish to black signal is found predominantly in the pit cells (pc) of the mouse LRO. (V) Cryosection of the embryo that previously underwent *in situ* hybridization using the probe directed against *Dnah9*. The white rectangle in V marks the region magnified in IV. (IV-V) Nuclei were counterstained with DAPI and are depicted in blue. Scale bars represent 50 μm (IV) or 5 μm (V).

(D) Comparison of expression profiles of genes encoding components of the outer dynein arm at five different time points of differentiation in ALI-cultured nasal epithelial cells. The RNA expression level is very low at early time points (t = 0 to t = 3) increasing heavily at later time points (t = 15) and slightly decreasing at t = 30. The differentiation-dependent expression profile of DNAH9 (in red) in ALI-cultured nasal epithelial cells resembles that of known outer dynein arm components.

identified individuals with loss-of-function mutations in *DNAH9* displayed laterality defects, we expect that loss of function of *DNAH9* leads to randomization of the left-right body asymmetry, resembling findings observed in individuals carrying recessive *DNAH5*,[28] *DNAH11*,[31,32] *DNAI1*,[29] and *DNAI2*[30] mutations. However, identification of individuals with loss-of-function mutations in *DNAH9* without laterality defects is difficult due to the fact that, in contrast to PCD caused by mutations in other genes, respiratory problems are less prominent and may not lead to thorough medical diagnostic work-up.

To test whether *DNAH9* expression is consistent with function in motile respiratory cilia, we quantified *DNAH9* expression in various cell types including Epstein-Barr-Virus-(EBV)-transformed lymphocytes (no motile cilia) (n = 2 healthy control individuals), blood cells (n = 3 healthy control individuals), nasal brushing biopsies (n = 3 healthy control individuals), and respiratory cells grown on air liquid interface (ALI) culture to full differentiation (n = 2 healthy control individuals). ALI-cell culture, transformation of lymphocytes using EBVs, and generation of human transcriptome profiles were performed as previously described.[41,42] Indeed, in agreement with a function of DNAH9 in motile cilia, we observed comparable *DNAH9* expression in nasal brushing biopsies and ALI-cultured nasal epithelial cells where hundreds of motile cilia per cell were present, whereas EBV-infected lymphocytes and blood cells lacking any motile cilia showed no or weak expression levels of *DNAH9* or other genes encoding ODA proteins (Figure S5). Furthermore, we observed upregulation of *DNAH9* expression during *in vitro* ciliogenesis of respiratory cells between day 3 and day 15, similar to the expression of other genes encoding ODA components (Figure 2D).

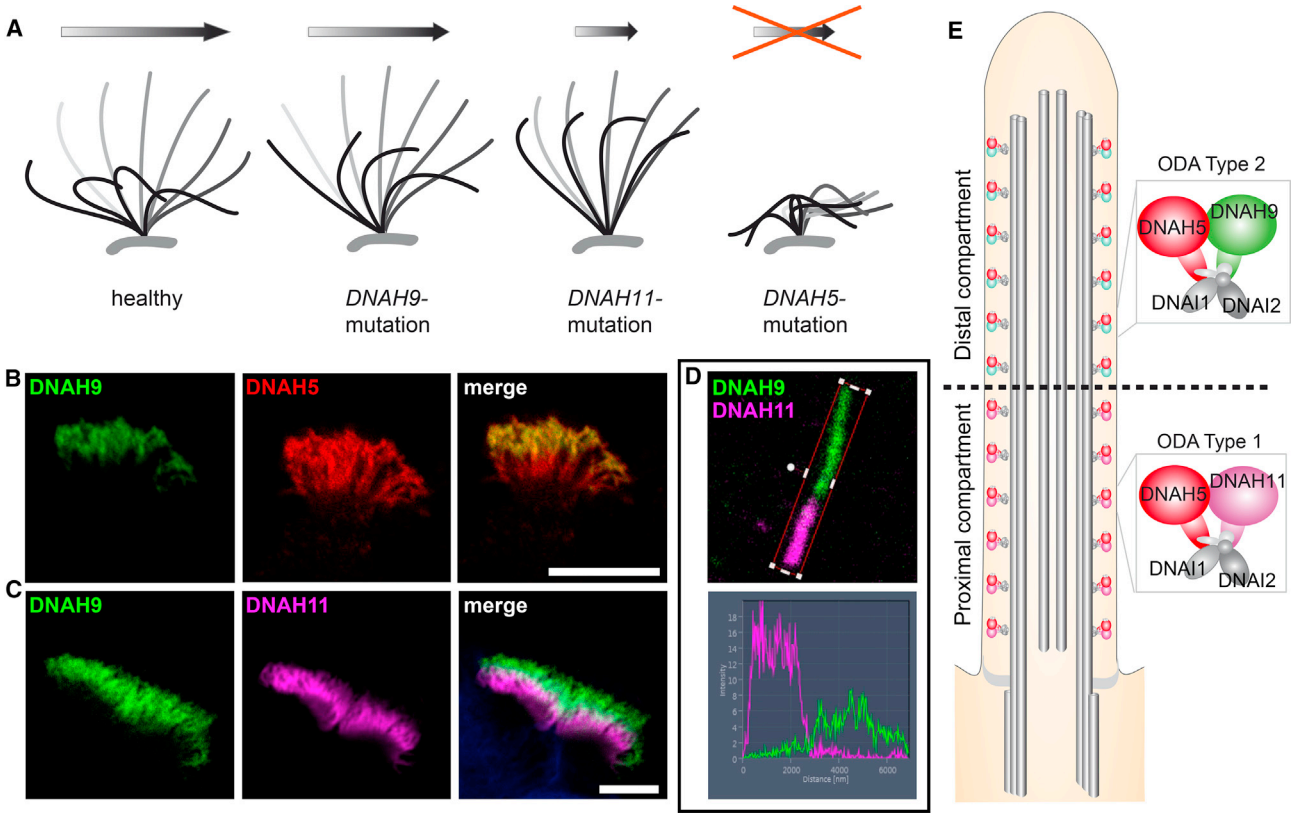

Figure 3. Schematics Depicting the Respective Aberrant Beating Patterns Caused by Recessive *DNAH9*, *DNAH11*, and *DNAH5* Mutations and Localization of the Axonemal Outer Dynein Arm β-Heavy Chains (ODA HC) DNAH9 and Paralogous DNAH11 and the ODA γ-HC DNAH5 in Respiratory Cilia

(A) Schematic of representative respiratory ciliary beating defects caused by loss-of-function mutations in *DNAH9*, *DNAH11*, and *DNAH5*. Whereas ciliary beating in healthy individuals demonstrate effective beating (gray) and recovery (black) strokes to move mucus in the airways (arrow), *DNAH9* and *DNAH11* mutant cilia show reduced bending in the distal and proximal ciliary regions, respectively. *DNAH5* mutant cilia are immotile with residual flickering movements.

(B and C) The ODA β-HC DNAH9 (green) localizes to the distal part of the ciliary axoneme and the ODA γ-HC DNAH5 (red) localizes to the whole ciliary axoneme. In contrast, the ODA β-HC DNAH11 (magenta) localizes to the proximal part of the ciliary axoneme. The overlapping front (white) results from the bending of the cilia. Scale bars represent 10 μm.

(D) Profiles of immunofluorescence intensity show an increase in the magenta signal in the proximal ciliary axoneme and an increase of the green signal in the distal ciliary axoneme. Both signals do not overlap indicating a distinct distal and proximal localization of β-heavy chain paralogs DNAH9 (green) and DNAH11 (magenta), respectively.

(E) ODA type 1 (DNAH5 and DNAH11) and ODA type 2 (DNAH5 and DNAH9) complexes define distinct compartments in respiratory cilia.

Previous studies of the orthologous ODA β-HC in the flagellated unicellular algae *Chlamydomonas reinhardtii* demonstrated an essential role for flagella movement.[3,43] To determine whether DNAH9 plays a similar role in human respiratory cells, we next investigated motile cilia function and structure in individuals with *DNAH9* mutations and we obtained nasal brush biopsies of three individuals: OP-2905 II1, OP-1226 II1, and MS-SI46 II1.

High-speed video microscopy of respiratory cells from individuals OP-2905 II1 and OP-1226 II1 revealed motile cilia with normal ciliary beat frequency (approx. 7 Hz at 25°C). However, we found abnormal beat pattern with reduced bending of the distal ciliary axoneme (Videos S1, S2, S3, and S4 and Figure 3A) when compared to controls (Video S5 and Figure 3A) consistent with DNAH9 localization and function in distal respiratory ciliary axonemes. The very subtle beating defect is also consistent with the observed mild respiratory symptoms in *DNAH9* mutant individuals. This ciliary beating defect appears to be more subtle when compared to defects caused by *DNAH11* and *DNAH5* mutations (Figure 3A and videos S6 and S7).

In control human respiratory cilia, DNAH9 localizes exclusively to the distal part of the respiratory ciliary axoneme while the β-DHC paralog DNAH11 localizes only to the proximal half. In contrast, DNAH5 shows a panaxonemal distribution along the ciliary axoneme[5,6] (Figures 3B–3E). To assess the effect of *DNAH9* variants on the axonemal localization of DNAH9 as well as localization of other ODA proteins, we performed high-resolution IF analysis of respiratory cilia obtained from individuals OP-2905 II1, OP-1226 II1, and MS-SI46 II1 and control subjects as previously described[44,45] using antibodies directed against the axonemal ODA heavy chains DNAH5, DNAH9, and DNAH11, the ODA intermediate

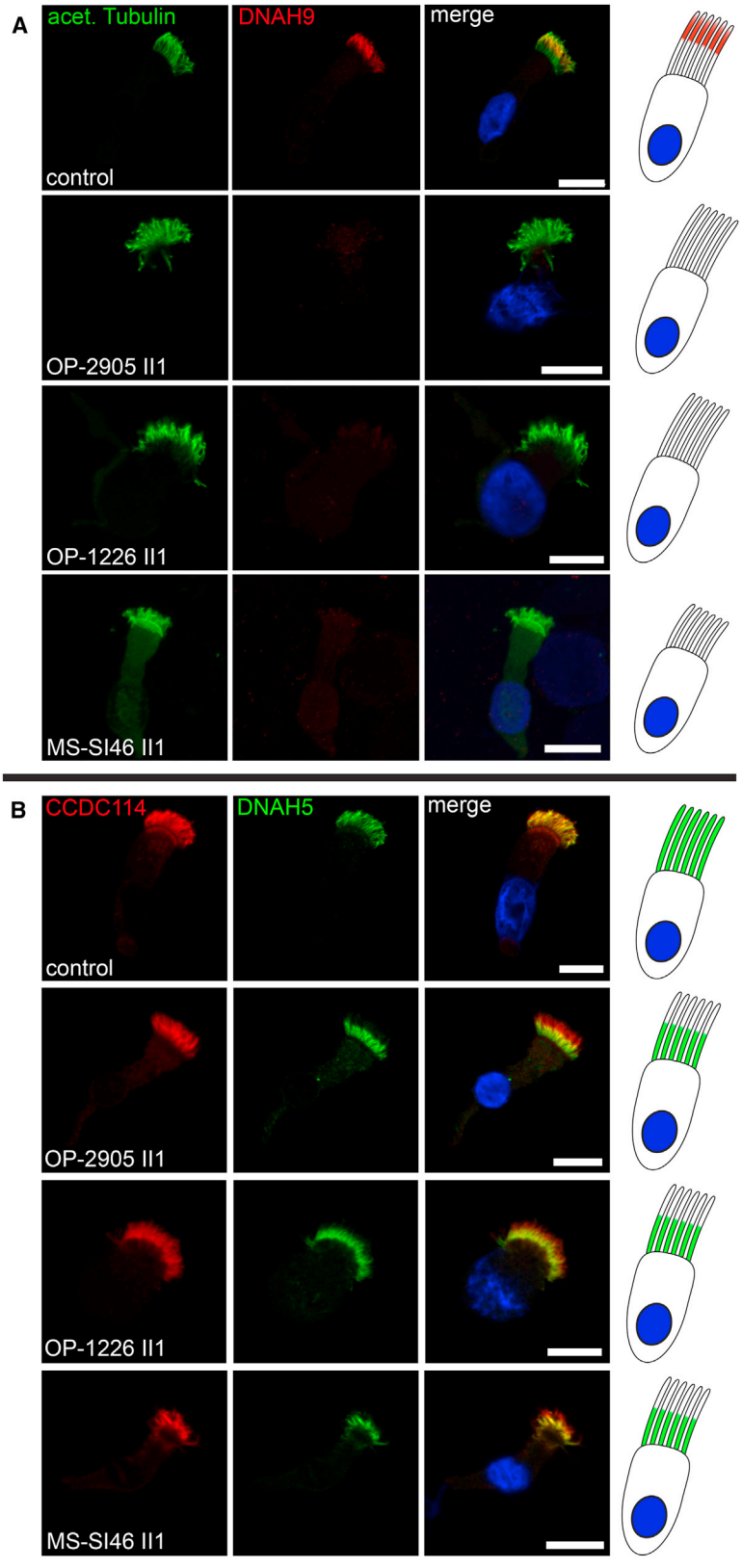

Figure 4. *DNAH9* Mutant Cilia Disrupt ODA Type 2 Complexes in the Distal Compartment of Respiratory Cilia

(A) In contrast to healthy control subjects, DNAH9 (red) is absent or severely reduced in the distal compartment of *DNAH9* mutant cilia. Ciliary axonemes are counterstained with anti-acetylated tubulin (green). Schematic (right side) highlights loss of DNAH9 (red) in the distal compartment of respiratory cilia.

(B) In contrast to healthy control subjects, DNAH5 (green) is absent or severely reduced in the distal compartment of *DNAH9* mutant cilia. DNAH5 retains localization in the proximal compartment of *DNAH9* mutant cilia. The ODA docking complex protein CCDC114 (red) localizes along the entire ciliary axoneme in both control and *DNAH9* mutant cilia. Schematic (right side) highlights loss of DNAH5 (green) in the distal compartment of respiratory cilia. Nuclei are stained with Hoechst33342 (blue). Scale bars represent 10 μm. For each individual, 15–20 cells were analyzed from two independent IF experiments.

chains DNAI1 and DNAI2, the ODA docking complex components TTC25 and CCDC114, as well as the N-DRC component GAS8. The anti-DNAH9 antibody (HPA052641, Atlas antibodies) recognizes an epitope that consists of amino acid residues 675–754. Consistent with loss-of-function mutations, DNAH9 was completely absent from the ciliary axoneme in OP-2905 II1, OP-1226 II1, and MS-SI46 II1 (Figure 4A). This indicates that despite moderately reduced scores predicted by Alamut for the wild-type splice site for the +4 splice site variant in OP-2905 II1, no wild-type transcript is present in multiciliated respiratory epithelial cells and probably the predicted alternative splice site causes a frameshift and/or the mRNA is subjected to nonsense-mediated decay. Additionally, DNAH5 was absent or severely reduced from the distal ciliary axoneme in all three individuals (Figures 4B and S6), and DNAI1 and DNAI2 were absent or severely reduced from the distal ciliary axonemes in individuals OP-2905 II1 and MS-SI46 II1 (Figures S7–S9). Cellular staining for ODA components such as DNAH5, DNAI1, and DNAI2 was also absent and results from protein degradation because ODA complexes cannot be correctly assembled in the cytoplasm and half-life of those components is shortened.[46] Thus, all three analyzed *DNAH9* mutant individuals depicted identical defects on the molecular (absence of DNAH9, DNAH5, DNAI1, and DNAI2) and sub-cellular (distal ciliary axoneme) levels. DNAH9 appears to be essential for assembly of ODAs type 2, because DNAH5 and DNAI2 are absent from the distal ciliary axonemes in *DNAH9* mutant cilia. Vice versa, we next analyzed the localization of DNAH9 in cells from PCD-affected individuals with mutations in *DNAH5*, *DNAI1*, *DNAI2*, and *DNAH11*. DNAH9 was absent from the distal ciliary

axonemes of *DNAH5*, *DNAI1*, and *DNAI2* mutant cilia (Figure 5), indicating that the ODA proteins DNAH5, DNAH9, DNAI1, and DNAI2 are components of the multimeric ODA type 2 in the distal ciliary axonemes and also essential for the assembly of distal ODAs type 2.

To gain insight into the spatiotemporal expression of the different ODA HC-proteins in human respiratory cilia, we then analyzed the localization of both β-ODA HCs DNAH9 and DNAH11 along the ciliary axonemes during ciliogenesis in control cells. Primary respiratory cell cultures and *in vitro* ciliogenesis experiments were performed as described in the Supplemental Methods. In early ciliogenesis stages (day 4–8) only DNAH11, but not DNAH9, is assembled into the ciliary axoneme. Between ciliogenesis day 10 and 12, we then observed localization of DNAH9 in the very distal ciliary axoneme, which extended during ciliogenesis (day 14) (Figure S10). Interestingly, Oltean et al. showed also an asynchronous expression/localization of both β-ODA HCs during ciliogenesis of respiratory cilia consistent with our findings.[47] In contrast, in *DNAH11* mutant cilia, DNAH9 is already present in short ciliary axonemes suggesting assembly at early stages of ciliogenesis and localization was panaxonemal in all analyzed ciliary axonemes independent of the cilia length (Figures 5, S11, and S12).[6] On the other hand, proximal DNAH11 localization was not altered in *DNAH9*, *DNAI2*, or *DNAH5* mutant respiratory cilia as well as *DNAAF2* and *DNAAF4* mutant respiratory cells (MIM: 612517 and 608706, respectively), indicating that DNAH11 evolved as a specific proximal β-ODA HC (Figures S13 and S14). Localization of the ODA docking complex proteins CCDC114 and TTC25 and the N-DRC component GAS8 was not affected in DNAH9-deficient ciliary axonemes (Figures 4B and S15). Thus, the assembly of the ODA docking complex and the N-DRC does not depend on DNAH9 function.

To further analyze the ciliary defect resulting from DNAH9 loss of function, we performed TEM as previously described[30] with samples of one *DNAH9* mutant individual who was available for analysis (OP-2905 II1). A total of 153 ciliary axonemes were analyzed. Confirming our high-resolution IF microscopy findings, ultrastructural analyses found ODAs to be absent from the distal ciliary axoneme and only ODA docking complexes were visible by TEM analyses of ciliary cross-sections of individual OP-2905 II1 (Figure 6A). Consistent with the restricted localization of DNAH9 to the distal part of the axoneme, outer dynein arms in the proximal ciliary axonemes were still present (Figure 6B). These findings confirm that mutations in *DNAH9* result in specific absence of ODAs type 2 and consequently result in an aberrant distal ciliary beating pattern. Usually, ODA defects documented by TEM or high-resolution IF are considered hallmark defects for PCD.[34] Thus, the report of three individuals without a classical PCD phenotype and absence of distal ODAs documented by high-resolution IF ($n = 3$) and TEM ($n = 1$) might be of interest for diagnostic testing in PCD.

To identify direct interaction partners of DNAH9, we then proceeded to perform yeast two-hybrid (Y2H) one-on-one screening as previously described.[42,48] We used eight different DNAH9 fragments due to the large cDNA and a customized prey protein grid containing known ODA components (such as DNAH5 fragments DNAI1 and DNAI2), ODA docking complex proteins, dynein axonemal assembly factors, inner dynein arm components, intraflagellar transport proteins, chaperones, and other proteins (Tables S3–S5). DNAH9 putative functional protein domains were taken into account to avoid splitting domains (Figure S16A, Table S4, and Supplemental Methods). We screened all eight DNAH9 fragments against the PCD protein grid and detected only one interaction: DNAH9 fragment 2 covering amino acids (aa) 201–859 containing the DHC domain 1 interacted with full-length CCDC114 (Figure S16B). None of the other DNAH9 fragments interacted with CCDC114 and we did not observe any interaction of any DNAH9 fragment with other proteins tested (Table S3). This included DNAH9 fragment 2 which did not interact with any other known proteins tested (Table S3, Figure S16B) excluding autoactivation of this fragment. Autoactivation of full-length CCDC114 had been previously excluded.[48] We confirmed this interaction by filter lift assay (Figure S16C) and subsequently by co-immunoprecipitation (Figures 7 and S17). Experimental details can be found in the Supplemental Methods. For co-immunoprecipitation experiments, in brief, 3xHA- as well as 3xFLAG-tagged proteins were transiently overexpressed in HEK293T cells and cells were harvested 48 hr after transfection. Co-immunoprecipitation was then performed as previously described.[42,48] In addition, we demonstrate that DNAH9 is absent from *CCDC114* mutant respiratory ciliary axonemes (Figure S18). Thus, the ODA docking complex component CCDC114 might be directly involved in docking of the distal ODAs type 2. Our immunofluorescence data demonstrated that DNAH9 is essential for ODA type 2 integrity. However, we did not detect a direct interaction of DNAH9 with DNAH5, DNAI2, or DNAI1 by Y2H. Y2H requires location of tested molecules in the nucleus which can result in failure to detect interactions. Further, the DNAH5 fragments we tested in the Y2H assay did not cover the full length of the protein (Figure S19A); fragmentation may have affected folding and thus binding to DNAH9. In addition, Y2H only detects direct interactions. We therefore decided to test interactions between DNAH9 and two of the other ODA proteins distally absent in DNAH9-deficient respiratory cilia, DNAH5 and DNAI2, using co-immunoprecipitation. We proceeded to subclone two larger *DNAH5* fragments covering also N-terminal areas uncovered in our Y2H screen: DNAH5 fragment 1 covering amino acid 1–1,807 including the DHC1 and DHC2 domain and DNAH5 fragment 2 covering amino acid 1,807–2,924 containing the D1 motor (ATPase domain) for expression in mammalian cells (Figure S19A). *DNAI2* full-length cDNA

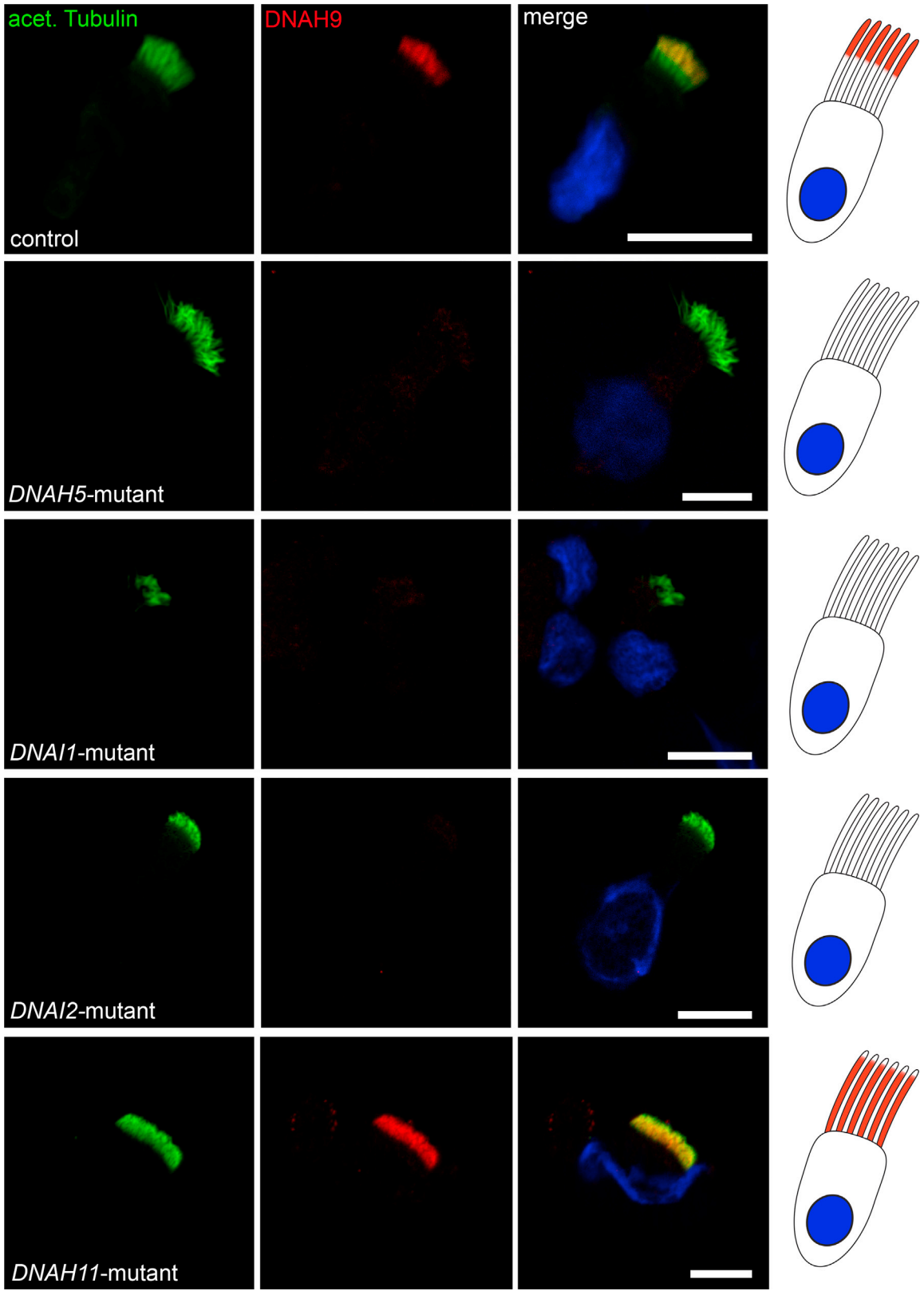

Figure 5. Mutations in *DNAH5*, *DNAI1*, *DNAI2*, and *DNAH11* Affect Axonemal Localization of DNAH9
Respiratory cilia double-labeled with antibodies directed against acetylated tubulin (green) and DNAH9 (red) show colocalization of DNAH9 with acetylated tubulin at the distal part of the cilia from an unaffected control (yellow). In contrast, DNAH9 is absent or severely reduced in *DNAH5*, *DNAI1*, and *DNAI2* mutant ciliary axonemes. Interestingly, in *DNAH11* mutant cilia the distal localization of DNAH9 shifts from distal to a panaxonemal localization. Nuclei were stained with Hoechst33342 (blue). Scale bars represent 10 μm. For each individual, 15–20 cells were analyzed.

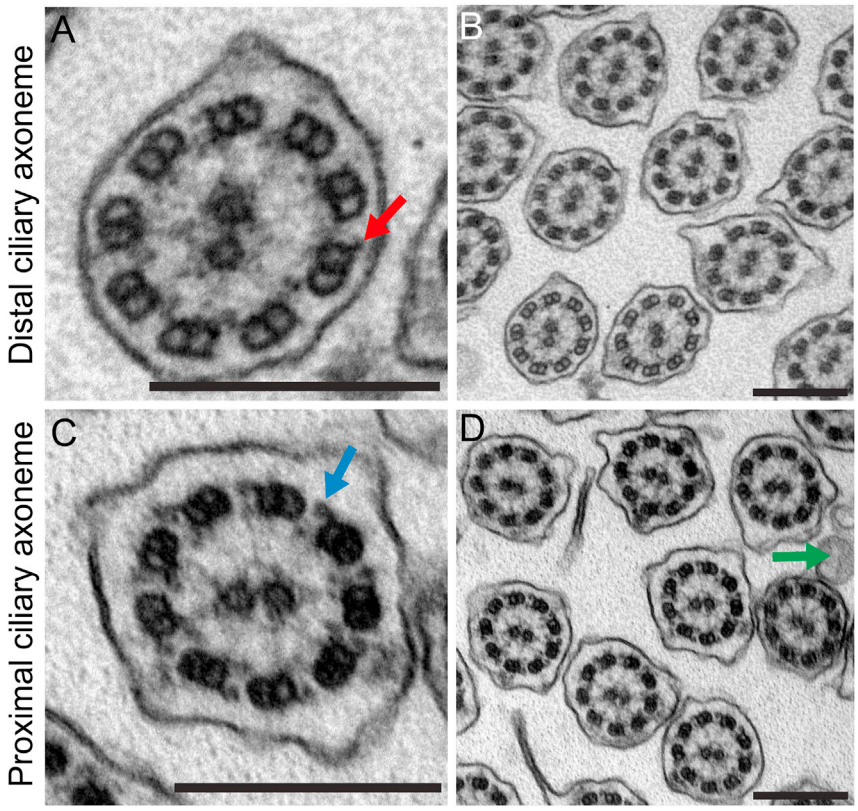

Figure 6. Distal Ciliary Axonemes of *DNAH9*-Deficient Respiratory Cells Display Subtle Ultrastructural Defects of the Outer Dynein Arms (ODAs)

(A and B) Loss-of-function mutations in *DNAH9* cause distal absence of ODAs in the transmission-electron microscopy but do not affect the ODA docking complex (DC) (red arrow in A).

(C and D) Interestingly, ODAs in the proximal part of the ciliary axonemes (blue arrow in C) are not affected by DNAH9 deficiency. The green arrow in (D) marks microvilli extending from the apical side of the cell.

Scale bars represent 200 nm. A total of 153 ciliary cross-sections were analyzed.

was also subcloned for expression in mammalian cells. For DNAH9, we focused on the fragments containing the DHC domains, as our Y2H result suggested that DHC domains could be important for protein-protein interactions. DNAH9 fragment localization is visualized in Figures 1B and S16A. Methodical details are described in the Supplemental Methods. Consistent with our high-resolution IF microscopy results, we found interaction of DNAH9 fragment 4 containing the DHC2 domain with both DNAH5 fragments and full-length DNAI2, indicating that DNAH9 is indeed interacting with ODA proteins localized in the distal ciliary axonemes (Figures S19B and S19C).

DNAH9, like other genes encoding axonemal dynein heavy chains, is a very large gene containing 69 coding exons encoding a 4,486-amino-acid protein. Consistent with laterality defects in *DNAH9* mutant individuals, we show by *in situ* hybridization that *Dnah9* is expressed in pit cells of the mouse embryonic ventral node (Figure 2C), indicating a role of DNAH9 in left-right patterning of the body axis similar to the ODA β-HC paralog DNAH11 and ODA γ-HC DNAH5.[6,28] During evolution, the gene encoding the ODA β-HC duplicated late during metazoan evolution at the origin of the Chordata[49,50] to produce three genes encoding ODA β-HCs in mammals. In human respiratory cilia, there are two different orthologs of the *Chlamydomonas* ODA β-HC, DNAH9 and DNAH11 (Figure S20), with distinct axonemal localization and most probably distinct functions. During metazoan evolution a third ODA β-HC emerged, DNAH17, which shows a distinct tissue distribution and seems to be important for sperm motility based on analyses of publicly available data bases for gene and protein expression (The Human Protein Atlas; GEO Profiles).

In the unicellular alga *Chlamydomonas reinhardtii*, the absence of the ODA β-HC causes swimming defects due to axonemal absence of the ODAs,[43] resembling findings observed in *DNAH9* mutant cells in which the ODA components DNAH5, DNAI1, and DNAI2 are absent from the distal ciliary axoneme. Furthermore, in *oda2*, *oda6*, and *oda9 Chlamydomonas reinhardtii* mutants (orthologs of *DNAH5*, *DNAI1*, and *DNAI2*, respectively), the absence of these components prevents assembly of the ODA β-HC.[3,51] Likewise, human mutations in genes encoding ODA components such as *DNAH5*, *DNAI1*, and *DNAI2* result in absence of DNAH9 from the distal ciliary axoneme[5,30] (Figure 5). These findings indicate that DNAH9 is a component of ODAs type 2 and assembly of DNAH9 is dependent on other ODA components resembling the function of the ancient *Chlamydomonas* ODA β-HC. In contrast, the paralogous ODA β-HC DNAH11 is localized in the proximal axonemal compartment of respiratory cilia and assembly of DNAH11 to the ciliary axoneme is probably independent from other ODA components such as DNAH5, DNAI1, and DNAI2 as its localization in these respective mutant cells is not affected[6] (Figure S13). We therefore propose that DNAH9 and DNAH11 developed specific compartmental function during evolution, reflected by their distinct axonemal localization and assembly. DNAH9 probably still functions similar to the ancient ODA β-HC of *Chlamydomonas* while DNAH11 developed distinct functions in mammalian in the proximal compartment of respiratory cilia.

In summary, we describe recessive loss-of-function mutations in *DNAH9* encoding the ODA β-HC DNAH9 as a cause for laterality defects without or with subtle symptoms of airway cilia dysfunction. The mild respiratory

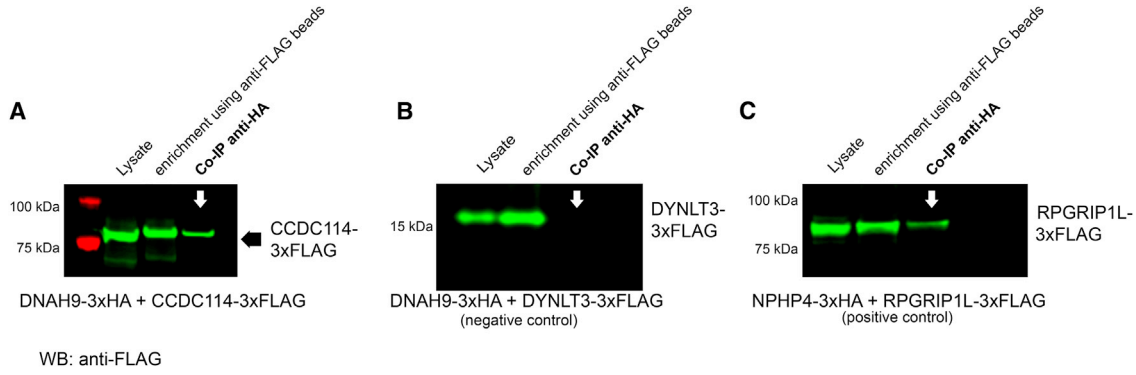

Figure 7. DNAH9 DHC Domain 1 Interacts with CCDC114
Co-immunoprecipitation (co-IP) confirmed the interaction between DNAH9 fragment 2 and CCDC114. HEK293T cells were transfected with DNAH9-fragment-2-3xHA and CCDC114-3xFLAG (A), DNAH9 fragment-2-3xHA, and DYNLT3-3xFLAG (B, negative control). NPHP4-3xHA and RPGRIP1L-C-term-3xFLAG were used as positive control (C). Co-IP was performed with the anti-HA antibody while anti-FLAG beads were used for enrichment. Western blot (WB) was performed using an antibody directed against the FLAG tag. DNAH9-fragment-2 was able to precipitate full-length CCDC114 (A) with protein amounts detected in the co-IP comparable to what we observe for the positive control (C) while no interaction between DNAH9-fragment-2 and DYNLT3 was observed (negative control) (B). Lysate shows protein content before pull down, enrichment shows pulled down prey protein.

phenotype results from only distally impaired axonemal bending, consistent with DNAH9 localization and distinct, distally restricted loss of ODA components. In parallel, Fassad et al. also found a reduction of ODA components in the distal ciliary compartment in individuals with recessive variants in DNAH9,[52] consistent with our findings. We conclude that DNAH9 is essential for ODA type 2 assembly and our data indicate that docking of ODAs type 2 occurs via direct interaction of DNAH9 with the docking complex protein CCDC114.

Supplemental Data

Supplemental Data include 20 figures, 6 tables, Supplemental Methods, and 7 videos and can be found with this article online at https://doi.org/10.1016/j.ajhg.2018.10.020.

Acknowledgments

We thank the PCD-affected individuals and their families for their participation and acknowledge the German PCD support group Kartagener Syndrom und Primaere Ciliaere Dyskinesie e.V. We thank A. Dorißen, D. Ernst, S. Helms, M. Herting, A. Robbers, L. Schwiddessen, F.J. Seesing, M. Tekaat, K. Wohlgemuth, and C. Westermann for excellent technical work. We also thank Dr. Alper Guzeltas, University of Health Sciences, Mehmet Akif Ersoy Thoracic and Cardiovascular Surgery Training and Research Hospital, Department of Pediatric Cardiology, 34303 Istanbul, Turkey and Dr. Helen Bornaun, Cardiology Department, Health Sciences University, Kanuni Sultan Suleyman Research and Training Hospital, Istanbul, Turkey for the diagnosis and referral of the individual MS_SI46 II.1 for genetic workup. The authors would like to thank the Genome Aggregation Database and the groups that provided exome variant data for comparison. A full list of contributing groups can be found at http://gnomad.broadinstitute.org/. This work was supported by the Deutsche Forschungsgemeinschaft OM6/7, OM6/8, OM6/10, and DFG KFO 326 (H. Omran), OL450/1 (H. Olbrich), and HJ7/1-1 (R.H.), by the IZKF Muenster to H. Omran (Om2/009/12 and Om/015/16), the European Union seventh FP under GA Nr. 305404, project BESTCILIA (H. Omran), and "Innovative Medical Research" of the University of Muenster Medical School to N.T.L. (I-LO121517). M.S. acknowledges funding from Radboudumc and RIMLS Nijmegen (Hypatia tenure track fellowship), the Deutsche Forschungsgemeinschaft (DFG CRC1140 KIDGEM), and the European Research Council (ERC StG TREATCilia, grant no. 716344).

Declaration of Interests

The authors have no competing interests to declare.

Received: May 29, 2018
Accepted: October 23, 2018
Published: November 21, 2018

Web Resources

1000 Genomes, http://www.internationalgenome.org/
Database of Genomic Variants, http://projects.tcag.ca/variation/
dbSNP, https://www.ncbi.nlm.nih.gov/projects/SNP/
ExAC Browser, http://exac.broadinstitute.org/
Galaxy, https://usegalaxy.org/
GEO Profiles, https://www.ncbi.nlm.nih.gov/geoprofiles/
gnomAD Browser, http://gnomad.broadinstitute.org/
HomozygosityMapper software, http://www.homozygositymapper.org/
HOPE, http://www.cmbi.ru.nl/hope
Human Splicing Finder, http://www.umd.be/HSF3/
NHLBI Exome Sequencing Project (ESP) Exome Variant Server, http://evs.gs.washington.edu/EVS/
OMIM, http://www.omim.org/
The Human Protein Atlas, http://www.proteinatlas.org/

References

1. Fliegauf, M., Benzing, T., and Omran, H. (2007). When cilia go bad: cilia defects and ciliopathies. Nat. Rev. Mol. Cell Biol. *8*, 880–893.

2. Porter, M.E., and Sale, W.S. (2000). The 9 + 2 axoneme anchors multiple inner arm dyneins and a network of kinases and phosphatases that control motility. J. Cell Biol. *151*, F37–F42.
3. Fowkes, M.E., and Mitchell, D.R. (1998). The role of preassembled cytoplasmic complexes in assembly of flagellar dynein subunits. Mol. Biol. Cell *9*, 2337–2347.
4. Pazour, G.J., Agrin, N., Walker, B.L., and Witman, G.B. (2006). Identification of predicted human outer dynein arm genes: candidates for primary ciliary dyskinesia genes. J. Med. Genet. *43*, 62–73.
5. Fliegauf, M., Olbrich, H., Horvath, J., Wildhaber, J.H., Zariwala, M.A., Kennedy, M., Knowles, M.R., and Omran, H. (2005). Mislocalization of DNAH5 and DNAH9 in respiratory cells from patients with primary ciliary dyskinesia. Am. J. Respir. Crit. Care Med. *171*, 1343–1349.
6. Dougherty, G.W., Loges, N.T., Klinkenbusch, J.A., Olbrich, H., Pennekamp, P., Menchen, T., Raidt, J., Wallmeier, J., Werner, C., Westermann, C., et al. (2016). DNAH11 localization in the proximal region of respiratory cilia defines distinct outer dynein arm complexes. Am. J. Respir. Cell Mol. Biol. *55*, 213–224.
7. Behan, L., Dimitrov, B.D., Kuehni, C.E., Hogg, C., Carroll, M., Evans, H.J., Goutaki, M., Harris, A., Packham, S., Walker, W.T., and Lucas, J.S. (2016). PICADAR: a diagnostic predictive tool for primary ciliary dyskinesia. Eur. Respir. J. *47*, 1103–1112.
8. Werner, C., Onnebrink, J.G., and Omran, H. (2015). Diagnosis and management of primary ciliary dyskinesia. Cilia *4*, 2.
9. Lin, A.E., Krikov, S., Riehle-Colarusso, T., Frías, J.L., Belmont, J., Anderka, M., Geva, T., Getz, K.D., Botto, L.D.; and National Birth Defects Prevention Study (2014). Laterality defects in the national birth defects prevention study (1998-2007): birth prevalence and descriptive epidemiology. Am. J. Med. Genet. A. *164A*, 2581–2591.
10. Morelli, S.H., Young, L., Reid, B., Ruttenberg, H., and Bamshad, M.J. (2001). Clinical analysis of families with heart, midline, and laterality defects. Am. J. Med. Genet. *101*, 388–392.
11. Kennedy, M.P., Omran, H., Leigh, M.W., Dell, S., Morgan, L., Molina, P.L., Robinson, B.V., Minnix, S.L., Olbrich, H., Severin, T., et al. (2007). Congenital heart disease and other heterotaxic defects in a large cohort of patients with primary ciliary dyskinesia. Circulation *115*, 2814–2821.
12. Nonaka, S., Tanaka, Y., Okada, Y., Takeda, S., Harada, A., Kanai, Y., Kido, M., and Hirokawa, N. (1998). Randomization of left-right asymmetry due to loss of nodal cilia generating leftward flow of extraembryonic fluid in mice lacking KIF3B motor protein. Cell *95*, 829–837.
13. McGrath, J., Somlo, S., Makova, S., Tian, X., and Brueckner, M. (2003). Two populations of node monocilia initiate left-right asymmetry in the mouse. Cell *114*, 61–73.
14. Tanaka, Y., Okada, Y., and Hirokawa, N. (2005). FGF-induced vesicular release of Sonic hedgehog and retinoic acid in leftward nodal flow is critical for left-right determination. Nature *435*, 172–177.
15. Simons, M., Gloy, J., Ganner, A., Bullerkotte, A., Bashkurov, M., Krönig, C., Schermer, B., Benzing, T., Cabello, O.A., Jenny, A., et al. (2005). Inversin, the gene product mutated in nephronophthisis type II, functions as a molecular switch between Wnt signaling pathways. Nat. Genet. *37*, 537–543.
16. Field, S., Riley, K.L., Grimes, D.T., Hilton, H., Simon, M., Powles-Glover, N., Siggers, P., Bogani, D., Greenfield, A., and Norris, D.P. (2011). Pkd1l1 establishes left-right asymmetry and physically interacts with Pkd2. Development *138*, 1131–1142.
17. Vetrini, F., D'Alessandro, L.C., Akdemir, Z.C., Braxton, A., Azamian, M.S., Eldomery, M.K., Miller, K., Kois, C., Sack, V., Shur, N., et al. (2016). Bi-allelic mutations in PKD1L1 are associated with laterality defects in humans. Am. J. Hum. Genet. *99*, 886–893.
18. Pennekamp, P., Karcher, C., Fischer, A., Schweickert, A., Skryabin, B., Horst, J., Blum, M., and Dworniczak, B. (2002). The ion channel polycystin-2 is required for left-right axis determination in mice. Curr. Biol. *12*, 938–943.
19. Bataille, S., Demoulin, N., Devuyst, O., Audrézet, M.P., Dahan, K., Godin, M., Fontès, M., Pirson, Y., and Burtey, S. (2011). Association of PKD2 (polycystin 2) mutations with left-right laterality defects. Am. J. Kidney Dis. *58*, 456–460.
20. Olbrich, H., Fliegauf, M., Hoefele, J., Kispert, A., Otto, E., Volz, A., Wolf, M.T., Sasmaz, G., Trauer, U., Reinhardt, R., et al. (2003). Mutations in a novel gene, NPHP3, cause adolescent nephronophthisis, tapeto-retinal degeneration and hepatic fibrosis. Nat. Genet. *34*, 455–459.
21. Gebbia, M., Ferrero, G.B., Pilia, G., Bassi, M.T., Aylsworth, A., Penman-Splitt, M., Bird, L.M., Bamforth, J.S., Burn, J., Schlessinger, D., et al. (1997). X-linked situs abnormalities result from mutations in ZIC3. Nat. Genet. *17*, 305–308.
22. Ma, L., Selamet Tierney, E.S., Lee, T., Lanzano, P., and Chung, W.K. (2012). Mutations in ZIC3 and ACVR2B are a common cause of heterotaxy and associated cardiovascular anomalies. Cardiol. Young *22*, 194–201.
23. Mohapatra, B., Casey, B., Li, H., Ho-Dawson, T., Smith, L., Fernbach, S.D., Molinari, L., Niesh, S.R., Jefferies, J.L., Craigen, W.J., et al. (2009). Identification and functional characterization of NODAL rare variants in heterotaxy and isolated cardiovascular malformations. Hum. Mol. Genet. *18*, 861–871.
24. Karkera, J.D., Lee, J.S., Roessler, E., Banerjee-Basu, S., Ouspenskaia, M.V., Mez, J., Goldmuntz, E., Bowers, P., Towbin, J., Belmont, J.W., et al. (2007). Loss-of-function mutations in growth differentiation factor-1 (GDF1) are associated with congenital heart defects in humans. Am. J. Hum. Genet. *81*, 987–994.
25. Guimier, A., Gabriel, G.C., Bajolle, F., Tsang, M., Liu, H., Noll, A., Schwartz, M., El Malti, R., Smith, L.D., Klena, N.T., et al. (2015). MMP21 is mutated in human heterotaxy and is required for normal left-right asymmetry in vertebrates. Nat. Genet. *47*, 1260–1263.
26. Paff, T., Kooi, I.E., Moutaouakil, Y., Riesebos, E., Sistermans, E.A., Daniels, H.J.M.A., Weiss, J.M.M., Niessen, H.H.W.M., Haarman, E.G., Pals, G., and Micha, D. (2018). Diagnostic yield of a targeted gene panel in primary ciliary dyskinesia patients. Hum. Mutat. *39*, 653–665.
27. Edelbusch, C., Cindrić, S., Dougherty, G.W., Loges, N.T., Olbrich, H., Rivlin, J., Wallmeier, J., Pennekamp, P., Amirav, I., and Omran, H. (2017). Mutation of serine/threonine protein kinase 36 (STK36) causes primary ciliary dyskinesia with a central pair defect. Hum. Mutat. *38*, 964–969.
28. Olbrich, H., Häffner, K., Kispert, A., Völkel, A., Volz, A., Sasmaz, G., Reinhardt, R., Hennig, S., Lehrach, H., Konietzko, N., et al. (2002). Mutations in DNAH5 cause primary ciliary dyskinesia and randomization of left-right asymmetry. Nat. Genet. *30*, 143–144.
29. Zariwala, M.A., Leigh, M.W., Ceppa, F., Kennedy, M.P., Noone, P.G., Carson, J.L., Hazucha, M.J., Lori, A., Horvath, J., Olbrich,

H., et al. (2006). Mutations of DNAI1 in primary ciliary dyskinesia: evidence of founder effect in a common mutation. Am. J. Respir. Crit. Care Med. *174*, 858–866.
30. Loges, N.T., Olbrich, H., Fenske, L., Mussaffi, H., Horvath, J., Fliegauf, M., Kuhl, H., Baktai, G., Peterffy, E., Chodhari, R., et al. (2008). DNAI2 mutations cause primary ciliary dyskinesia with defects in the outer dynein arm. Am. J. Hum. Genet. *83*, 547–558.
31. Knowles, M.R., Leigh, M.W., Carson, J.L., Davis, S.D., Dell, S.D., Ferkol, T.W., Olivier, K.N., Sagel, S.D., Rosenfeld, M., Burns, K.A., et al.; Genetic Disorders of Mucociliary Clearance Consortium (2012). Mutations of DNAH11 in patients with primary ciliary dyskinesia with normal ciliary ultrastructure. Thorax *67*, 433–441.
32. Schwabe, G.C., Hoffmann, K., Loges, N.T., Birker, D., Rossier, C., de Santi, M.M., Olbrich, H., Fliegauf, M., Failly, M., Liebers, U., et al. (2008). Primary ciliary dyskinesia associated with normal axoneme ultrastructure is caused by DNAH11 mutations. Hum. Mutat. *29*, 289–298.
33. Hornef, N., Olbrich, H., Horvath, J., Zariwala, M.A., Fliegauf, M., Loges, N.T., Wildhaber, J., Noone, P.G., Kennedy, M., Antonarakis, S.E., et al. (2006). DNAH5 mutations are a common cause of primary ciliary dyskinesia with outer dynein arm defects. Am. J. Respir. Crit. Care Med. *174*, 120–126.
34. Barbato, A., Frischer, T., Kuehni, C.E., Snijders, D., Azevedo, I., Baktai, G., Bartoloni, L., Eber, E., Escribano, A., Haarman, E., et al. (2009). Primary ciliary dyskinesia: a consensus statement on diagnostic and treatment approaches in children. Eur. Respir. J. *34*, 1264–1276.
35. Marthin, J.K., and Nielsen, K.G. (2013). Hand-held tidal breathing nasal nitric oxide measurement–a promising targeted case-finding tool for the diagnosis of primary ciliary dyskinesia. PLoS ONE *8*, e57262.
36. Jackson, C.L., Behan, L., Collins, S.A., Goggin, P.M., Adam, E.C., Coles, J.L., Evans, H.J., Harris, A., Lackie, P., Packham, S., et al. (2016). Accuracy of diagnostic testing in primary ciliary dyskinesia. Eur. Respir. J. *47*, 837–848.
37. Beydon, N., Chambellan, A., Alberti, C., de Blic, J., Clément, A., Escudier, E., and Le Bourgeois, M. (2015). Technical and practical issues for tidal breathing measurements of nasal nitric oxide in children. Pediatr. Pulmonol. *50*, 1374–1382.
38. Leigh, M.W., Hazucha, M.J., Chawla, K.K., Baker, B.R., Shapiro, A.J., Brown, D.E., Lavange, L.M., Horton, B.J., Qaqish, B., Carson, J.L., et al. (2013). Standardizing nasal nitric oxide measurement as a test for primary ciliary dyskinesia. Ann. Am. Thorac. Soc. *10*, 574–581.
39. Wallmeier, J., Shiratori, H., Dougherty, G.W., Edelbusch, C., Hjeij, R., Loges, N.T., Menchen, T., Olbrich, H., Pennekamp, P., Raidt, J., et al. (2016). TTC25 deficiency results in defects of the outer dynein arm docking machinery and primary ciliary dyskinesia with left-right body asymmetry randomization. Am. J. Hum. Genet. *99*, 460–469.
40. Downs, K.M., and Davies, T. (1993). Staging of gastrulating mouse embryos by morphological landmarks in the dissecting microscope. Development *118*, 1255–1266.
41. Munye, M.M., Shoemark, A., Hirst, R.A., Delhove, J.M., Sharp, T.V., McKay, T.R., O'Callaghan, C., Baines, D.L., Howe, S.J., and Hart, S.L. (2017). BMI-1 extends proliferative potential of human bronchial epithelial cells while retaining their mucociliary differentiation capacity. Am. J. Physiol. Lung Cell. Mol. Physiol. *312*, L258–L267.
42. Höben, I.M., Hjeij, R., Olbrich, H., Dougherty, G.W., Nöthe-Menchen, T., Aprea, I., Frank, D., Pennekamp, P., Dworniczak, B., Wallmeier, J., et al. (2018). Mutations in C11orf70 cause primary ciliary dyskinesia with randomization of left/right body asymmetry due to defects of outer and inner dynein arms. Am. J. Hum. Genet. *102*, 973–984.
43. Porter, M.E., Knott, J.A., Gardner, L.C., Mitchell, D.R., and Dutcher, S.K. (1994). Mutations in the SUP-PF-1 locus of *Chlamydomonas reinhardtii* identify a regulatory domain in the beta-dynein heavy chain. J. Cell Biol. *126*, 1495–1507.
44. Tarkar, A., Loges, N.T., Slagle, C.E., Francis, R., Dougherty, G.W., Tamayo, J.V., Shook, B., Cantino, M., Schwartz, D., Jahnke, C., et al.; UK10K (2013). DYX1C1 is required for axonemal dynein assembly and ciliary motility. Nat. Genet. *45*, 995–1003.
45. Omran, H., and Loges, N.T. (2009). Immunofluorescence staining of ciliated respiratory epithelial cells. Methods Cell Biol. *91*, 123–133.
46. Mitchison, H.M., Schmidts, M., Loges, N.T., Freshour, J., Dritsoula, A., Hirst, R.A., O'Callaghan, C., Blau, H., Al Dabbagh, M., Olbrich, H., et al. (2012). Mutations in axonemal dynein assembly factor DNAAF3 cause primary ciliary dyskinesia. Nat. Genet. *44*, 381–389.
47. Oltean, A., Schaffer, A.J., Bayly, P.V., and Brody, S.L. (2018). Quantifying ciliary dynamics during assembly reveals stepwise waveform maturation in airway cells. Am. J. Respir. Cell Mol. Biol. *59*, 511–522.
48. Hjeij, R., Onoufriadis, A., Watson, C.M., Slagle, C.E., Klena, N.T., Dougherty, G.W., Kurkowiak, M., Loges, N.T., Diggle, C.P., Morante, N.F., et al.; UK10K Consortium (2014). CCDC151 mutations cause primary ciliary dyskinesia by disruption of the outer dynein arm docking complex formation. Am. J. Hum. Genet. *95*, 257–274.
49. Kollmar, M. (2016). Fine-tuning motile cilia and flagella: evolution of the dynein motor proteins from plants to humans at high resolution. Mol. Biol. Evol. *33*, 3249–3267.
50. Wilkes, D.E., Watson, H.E., Mitchell, D.R., and Asai, D.J. (2008). Twenty-five dyneins in Tetrahymena: A re-examination of the multidynein hypothesis. Cell Motil. Cytoskeleton *65*, 342–351.
51. Piperno, G., and Luck, D.J. (1982). Outer and inner arm dyneins from flagella of *Chlamydomonas reinhardtii*. Prog. Clin. Biol. Res. *80*, 95–99.
52. Fassad, M., R., Shoemark, A., Legendre, M., Hirst, R.A., Koll, F., Le Borgne, P., Louis, B., Daudvohra, F., Patel, M.P., Thomas, L., et al. (2018). Mutations in outer dynein arm heavy chain DNAH9 cause motile cilia defects and situs inversus. Am. J. Hum. Genet. *103*, this issue, 984–994.